Journal of the European Ceramic Society 16 (1996) 301–314

0955-2219(95)00189-1
0955-2219/96/$15.00

Sol–gel Mullite Matrix-SiC and -Mullite 2D Woven Fabric Composites with or without Zirconia Containing Interphase: Elaboration and Properties

Ph. Colomban,[a]* E. Bruneton,[a,b] J. L. Lagrange[a] & E. Mouchon[a]

[a]ONERA-OM, BP 72, 92322 Chatillon, France
[b]CNRS-CECM, 15 rue G. Urbain, 94407 Vitry-sur-Seine, France

(Received September 1994; accepted 30 October 1995)

Abstract

The properties of composites made with fabrics of Nicalon® NLM202 SiC or Nextel® 440 mullite fibers are reported. The method used to make composites is a three stages sol–gel process: (i) in situ *gelation of a mixture of alkoxides in a ceramic fiber fabric; (ii) the deposit of a matrix precursor onto the impregnated fabrics and (iii) hot-pressing of the stacked fabrics in a carbon mold. The composites have been studied by SEM and TEM. Three point flexural strength has been measured at room temperature and at 900°C in air. Local Young's modulus, microhardness and interfacial shear stress have been determined at RT. Micro-Raman spectra and X-ray microanalysis have been used to study the fiber–interface reactions. Using a mixture of aluminium–silicon ester and tributylborate as interface precursor, we obtained a carbon film free SiC-mullite sliding interface. The use of a complementary ZrO_2–GeO_2 gel interface precursor allows us to obtain dense composites at a low temperature exhibiting good mechanical properties (linear behaviour up to ~180 MPa, even after annealing in air). The effects of a zirconia interphase on the mechanical properties of mullite–mullite composite are also discussed.*

Introduction

Many advanced aerospace systems require or would benefit from new low density materials for structural applications. Ceramic materials could replace existing metals and alloys, especially in corrosive environments. This is particularly true of those applications requiring materials working at temperatures above 800°C, e.g. aircraft engine parts. For these applications the most promising class of new materials is ceramic woven fabric-reinforced ceramic matrix composites. The use of monolithic ceramics is limited by their intrinsic inability to tolerate mechanical damage without brittle rupture due to their polycrystalline state and the nature of the chemical bonds existing in these compounds. The use of long, continuous ceramic fibers embedded in a refractory ceramic matrix results in a composite material exhibiting enhanced toughness through a specific micromechanism at the fiber–matrix interface: the cracks appearing in the matrix are deflected, dissociated and then stopped at the fiber–matrix interface. Thus the composite materials exhibit a pseudo-plastic fracture easily observed in the load–strain plots. Calculations with safety coefficients would thus be possible for parts made of ceramic matrix composites as well the manufacture of complex architectures. For aerospace applications requiring high reliability, it is necessary to use woven ceramic fibers as reinforcement. At present, Nicalon® NLM202 SiC fibers are considered to be the most convenient fibers but mullite fibers such as Nextel® 440 also present some potential advantages in the preparation of composites exhibiting both good thermomechanical properties and oxidation resistance. One of the most interesting matrices is mullite. The interest in the mullite matrix arises from its superb thermal and chemical stability and from its relatively low temperature expansion, comparable with that of the fibers. Furthermore, its mechanical properties, up to 1300–1500°C are retained. Also, its low toughness and Young's modulus can be improved by zirconia dispersion.

Improvements can be made using the sol–gel method, which allows refractory oxide matrices such as mullite, alumina, zirconia[1,2] to be processed

*To whom correspondence should be addressed. Also at CNRS-LASIR, 2 rue Henry Dunant, 94320 Thiais, France.

at relatively low temperatures (1000–1300°C) and fine grained ceramics to be produced with regular submicronic zirconia dispersion.[3] Finally, as these matrices are free of alkali- or alkaline-earth ions, there is no formation of a carbon rich interface at the boundary of the Nicalon SiC fiber.[4] This absence of a carbon film prevents rapid thermal degradation in oxidizing atmospheres. The reaction between the oxide fiber and the matrix has to be controlled in order to prevent the formation of a strong interfacial bond. In spite of the potential interest of mullite as a matrix for use in more or less oxidizing atmospheres, attempts to prepare long fiber reinforced mullite matrix composites remain limited. Jones *et al.*[5] and Qui & Pantano[6] have prepared mullite matrix composites using long SiC and carbon fibers. To date no work has been reported on the preparation and properties of woven fabric reinforced mullite matrix composites, except our preliminary reports of Refs 4 and 7.

In this paper we compare the properties of ceramic composites consisting of Nicalon® NLM202 (Nippon Carbon) SiC or with Nextel® 440 (3M) mullite fibers in mullite matrices, before and after annealing in air at temperatures between 900 and 1300°C. Emphasis is given on understanding the mechanical behaviour of each composite component: the fiber, the matrix and the fiber/matrix interface and interphases.

Experimental

Composite preparation

Our preparation process of two-dimensional (2D) woven fabric reinforced composites is based on the hydrolysis–polycondensation of alkoxides according to the following reaction

$$MOR_n + H_2O \rightarrow M(OR)_{n-1}(OH) + ROH$$

The resulting material is a gel (composition: $MO_{n-2x}(OH)_x mH_2O$) which is converted by thermal treatment into a meso/microporous 'glass' and then, after the departure of the last OH^-, densification leads to a glass, a glass-ceramic or a ceramic depending on composition.[1,2,8] The CMC's preparation process takes place in three stages (Fig. 1):

(i) impregnation of the fiber yarn of the fabrics with an interface fiber–matrix precursor (a liquid alkoxide mixture which slowly hydrolyses and polycondenses, *in situ* by reaction with air moisture into a gel);

(ii) deposition of the fine amorphous and reactive–matrix precursor (a gel powder which has been converted by thermal treatment at ca. 600–800°C in a mesoporous xerogel in order to evacuate most of the water in the polymeric network and hence to reduce the shrinkage). This powder precursor is deposited onto the interface precursor impregnated fabric in the form of a suspension in chlorobenzene, with addition of PMMA;

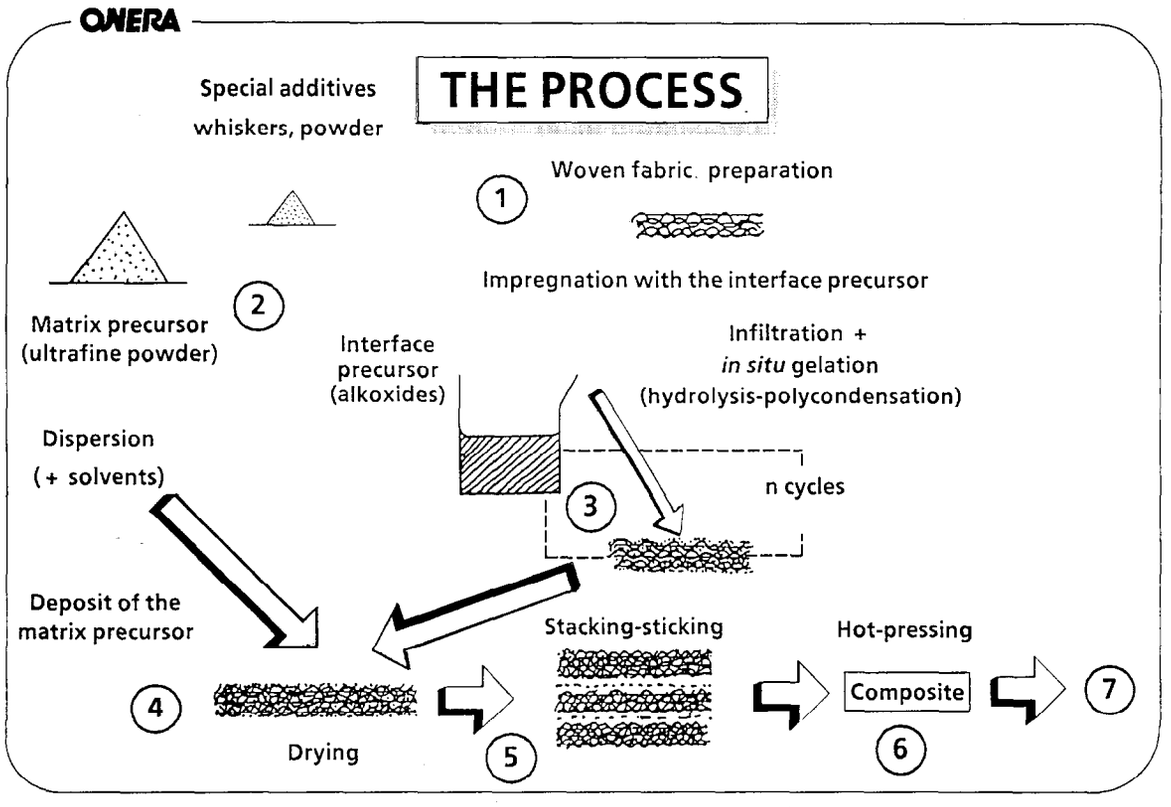

Fig. 1. Flowchart of the sol–gel route for the manufacture of ceramic fiber woven fabric–ceramic matrix composites.

(iii) hot pressing of the impregnated and stacked fabrics in a graphite mold at a temperature between 1000 and 1400°C.

Details on the manufacturing technology are given in Ref. 9.

The problems arising in the preparation of refractory matrix dense composites leads to the difficulty of achieving an open porosity below 8–10%. The fiber must be thoroughly embedded in the matrix and the matrix must be incorporated through the voids between fibers (a few microns or less, in size). This is possible by infiltration of liquid or gaseous precursors for which the ceramic yield is necessarily low. It results in considerable shrinkage which generates new voids: the presence of the woven fabrics inhibits the coherent shrinkage of the matrix. The ceramic precursor can infiltrate the yarns reducing the porosity and the shrinkage creates voids. In the case of two-dimensional reinforcement: this dilemma is solved by the use of a very reactive matrix precursor in association with a liquid interface precursor which polycondenses within the fiber yarns into a gel. On heating, the gel is converted in glass-ceramic and gives rise to a temporary liquid sintering aid at the same temperature at which the matrix densification occurs.[8] The liquid phase contributes to the densification by mass transport (liquid assisted sintering) but also helps to lubricate the powder rearrangement under pressure and to achieve a good contact between the grains coming from the matrix precursor and/or from the interface precursor despite the presence of a fiber network (Fiber volume: ~30–40%).

The matrix precursor is prepared by rapid hydrolysis of an alkoxide mixture diluted in propanol with very strong stirring.[1] The resulting gel is dried under IR bulbs and heated up to 750°C to reach the amorphous state. Densification occurs at about 1000°C for mullite with the dehydroxylation–nucleation–densification reaction.[8,10,11]

Woven fabrics

Nicalon® NLM202 fibers (Nippon Carbon Co.) were woven by CRST (21350 Gissey, France) along four directions in the plane to give a ~1 mm thick fabric (surface mass: 76×10^{-3} g/cm^{-1}). The SiC fiber diameter is ~15 μm and the thermal expansion of fiber is about $3–3{\cdot}5 \times 10^{-6}$ K^{-1}.[10] Yarns contain ~500 fibers.

Nextel® 440 mullite fiber (3M Co) were woven by Ets Cotton Frères (France) along two directions, within the plane to give a ~0·4 mm thick satin (surface mass: 22×10^{-3}/cm^2). The mullite fiber diameter is about 11 μm and a yarn contains 390 fibers. The thermal expansion is about 5×10^{-6} K^{-1}.

Interface precursors

Different kinds of interface precursors (so-called because the fiber–matrix interface will result from the reaction between the fibers and the precursor) may be used, solely or in combination, depending on the matrix and the fibers.[9,12] In the case of mullite matrix composites three different precursors are used:

(i) a mixture of $(OBu)_2$–Al–O–Si$(OEt)_2$ ester (ref. SiAl084 Dynasyl, from formely Dynamit Nobel, now Hüls-France) and tributylborate (TBB, from Alfa-Ventron, ref. 10691), or tributylphosphate $PO(O_tC_4H_9)_3$ (TBP from Fluka, ref. 10138);

(ii) pure zirconium i-propoxide (ZP, ref. 88733 from Fluka);

(iii) a mixture of ZP and tetra-ethoxy-germane (TEOGe, prepared at the laboratory).

The transient liquid sintering aid results from the melting of B_2O_3 (~600°C), Ge and of GeO_2 (~1100°C), both liquids being eliminated by volatilization during the hot-pressing cycle or incorporated in the matrix. It is important that no traces remain present at the grain boundaries in order to maintain good mechanical properties at high temperatures or in water-rich atmospheres.

Mullite matrix

A mullite matrix reinforced with a dispersion of zirconia is prepared by instant hydrolysis of a mixture of ZP and aluminum isobutoxide and silicon methoxide diluted in propanol as described in Ref. 13. A submicronic dispersion of tetragonal zirconia is obtained, (Fig. 2). The great advantage of the alkoxide route is that it blends the liquid gel-formers very homogeneously and keeps this homogeneity up to the nucleation at about 1000°C.[1,3] The steady size of the precipitates whatever the thermal treatment time is due to the low diffusion coefficient in the mullite glass-ceramic below 1400°C. The equilibrium between the crystallites and the host amorphous or spinel-like matrix depends only on temperature and composition.[3,11,14]

Hot pressing

Pressure sintering is performed under vacuum up to 400°C, a N_2 atmosphere (1 atm) being applied above 400°C. The heating rate is 250°C/h up to 600°C and increased to 350°C/h up to the dwell temperature. A pressure of 2·5 MPa is applied at the begining of the hot-pressing cycle in order to get a good contact between the fiber yarns and the interphase and matrix precursors. The applied pressure is then raised to 20 MPa between 600 and 900°C, this maximum value being reached before the beginning of the mullite intrinsic shrinkage (~850°C), related to the dehydroxylation–

nucleation reaction;[8,11] the pressure is removed just before the end of the dwelling time. Cooling is complete after 5 h.

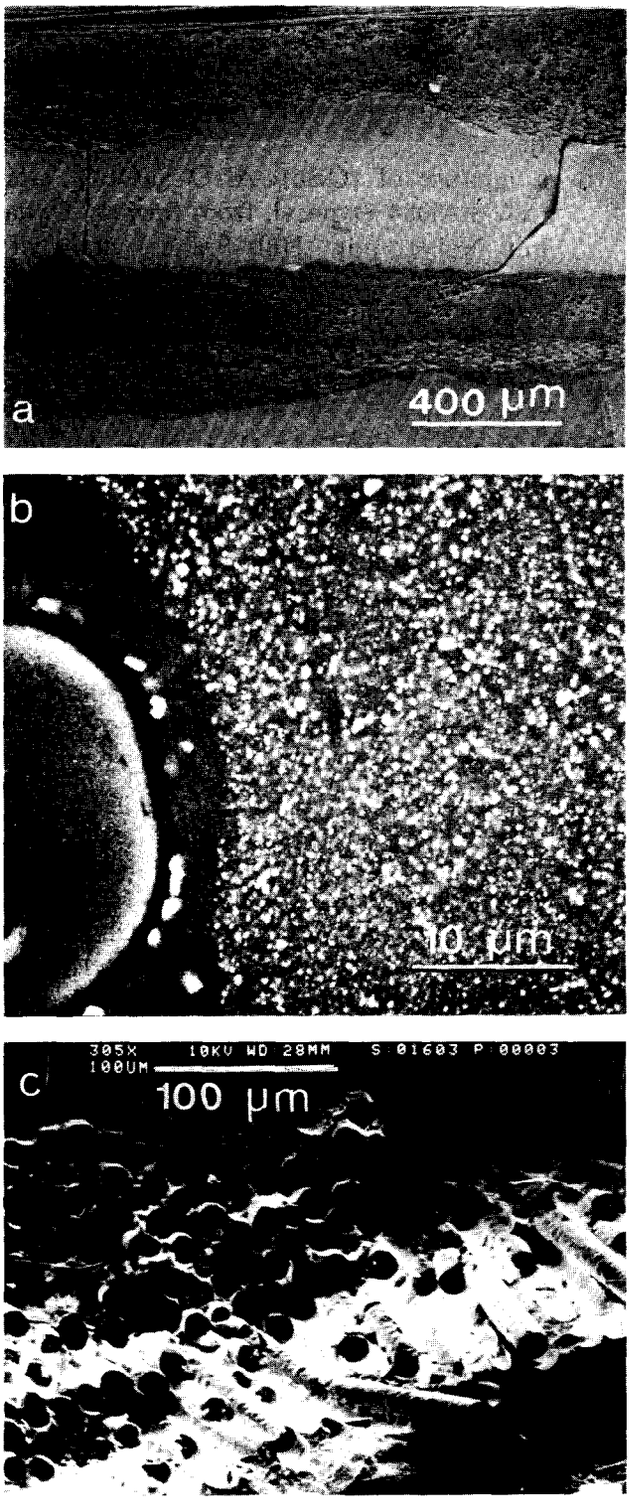

Fig. 2. Photomicrograph of a Nicalon NLM202® SiC fiber woven fabric–mullite matrix composites pressure sintered at 1350°C: (a) polished section: a regular $3Al_2O_32SiO_2$ matrix cracking pattern is observed, mean intercrack distance ~1 mm; (b) detail of the fiber–matrix interface; the zirconia precipitates of the matrix appear in white (mean matrix composition: $6Al_2O_34SiO_2{\cdot}ZrO_2$). The zirconia-free interphase around the SiC fiber arises from the transformation of the interface precursor deposit TBB+3SiAl (mean composition: $Al_2O_32SiO_2$ with B_2O_3 traces); (c) fracture of a Nextel 440 fiber fabric–mullite matrix composite pressure sintered at 1200°C (interface precursor: TBP+SiAl).

Interface precursor–matrix precursor reaction

Figure 2 gives an illustration of the interphase formation between the fiber and the matrix. The matrix composition was chosen to be $6Al_2O_3$ $4SiO_2{\cdot}ZrO_2$. The interface precursor is the mixture of TBB and SiAl ester (oxide composition: $Al_2O_32SiO_2nB_2O_3$). We can observe the homogeneous, submicronic dispersion of zirconia precipitates in the mullite matrix and a zirconia free contour around the SiC fiber can be observed (zirconia appears white in the SEM photomicrograph due to the high number of electrons of Zr). The contour corresponds to a silica-rich mullite glass-ceramic with nanometric mullite crystals created by the pyrolysis of the interface precursor gel. However, some zirconia crystals are observed at the fiber periphery because of zirconia precipitation through reaction with the temporary liquid sintering aid.

Techniques

The expansion measurement was achieved using an Adamel Lhormargy DI24 apparatus (Instrument SA, Longjumeau, France) with silica glass rod and support. Dilatometric curves were drawn under vacuum at heating and cooling rates of 5°C/min from room-temperature up to 900°C. Sample dimensions were $25 \times 10 \times 10$ mm^3.

Flexural strength was recorded by three point bending tests using a bar specimen (35 or 50 mm length) over a 30 mm span at a cross-head speed of 0·1 mm/min. Tests were performed at room temperature and at 900°C in air after 30 min stabilization (heating rate 300°C/h). Typically three samples were broken for each composition at both temperatures.

Fracture surfaces and sliced or polished sections of the samples were observed using an optical microscope or by scanning electron microscopy (Cambridge Scan 200 KV). TEM investigations were performed using 200 KV microscopes (Jeol 2000 FX and Topcon 002-B) both equipped with EDX analysis with optimal 5 nm spatial resolution. The standardless metallurgical thin film (SMTF) method was used to determine the local composition.

Local Young's modulus, microhardness and interfacial frictional stress (IFS:τ) were determined using a home-made Vickers microindenter instrument and models described in Ref. 15. The load cell measures loads up to 1 N with an accuracy of about 500 μN. The capacitive displacement gauge has an accuracy of some nanometers. The loading rate is load-controlled and varies from 7 to 30 mN/s. The position of the indenter relative to the polished surface of the sample and the applied

load were measured continuously during testing. This enables the hardness and Young's modulus to be determined without the need for direct imaging of the indentation. However, the size and shape of the indentation were always checked afterwards and the indentation axis position was checked using the method described in Ref. 15.

Micro-Raman spectra were recorded at the 514·5 nm exciting wavelength of an Ar^+ laser using a XY Dilor multichannel microprobe (Lille, France) equipped with a liquid nitrogen cooled Wright CCD (1200-300) array detector.

Results and Discussion

Porosity and macroscopic mechanical properties

SiC-mullite composites

Preliminary work has shown that 2D fabric SiC fiber/mullite matrix composites prepared by the above method exhibit a RT dissipative fracture (Fig. 3) and a rather good linear limit of strength behavior when a 1TBB + 3SiAl (volume ratio) interface precursor was used.[7] On the other hand, the deposit only the TBB precursor leads to a brittle composite.[16] Optimisation of the enduction process lowers the open porosity to about 9% and

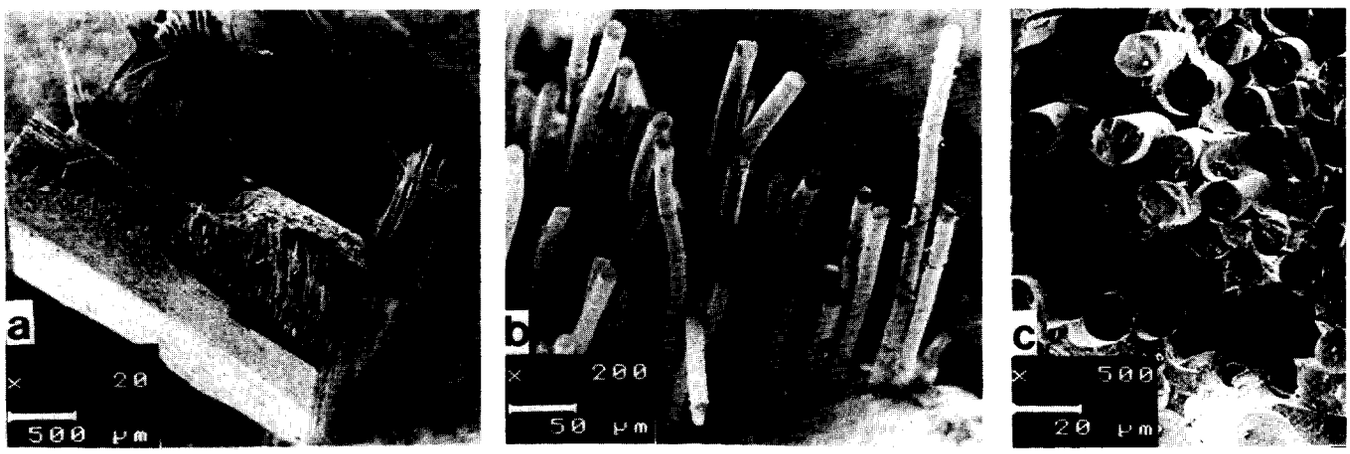

Fig. 3. Photomicrograph of a SiC fiber woven fabric-mullite matrix composite pressure sintered at 1350°C (TBB+3SiAl interface precursor). Fiber volume: 0·3; open porosity: 12%: (a) fracture at RT; (b) detail of the fiber pull-out at RT, and (c) after 900°C.

Table 1. Open porosity (P) and flexural strength (σ) of composites prepared using various interface and matrix precursors

Fabrics (fibers)	*Matrix*	*Interface precursors[c] (volume ratio)*	*Sintering temperature and dwell-time*	*σ (MPa)[d]*	*P (%)*
4 dir (NLM202)[a]	$3Al_2O_3{\cdot}2SiO_2$	TBB	1350°C (45 min)	<100 (brittle)[e]	~15
	$6Al_2O_3{\cdot}4SiO_2$ ZrO_2	1TBB 3SiAl	1350°C 45 min	~120–130 (100)[f] (dissipative)[e]	9–14
			1300°C 90 min	~150–180 (120)[f] (dissipative)[e] 150 µm	9
		1ZP 1TEOGe + 1TBB 3SiAl	1300°C 90 min	RT ~260 ± 30 900°C ~280 ± 20 (190)[f] (dissipative)[e] 500–2000 µm	3 ± 0·5
Satin (Nextel 440®)[b]	$3Al_2O_3{\cdot}2SiO_2$ $0.1TiO_2$	1SiAl + 1TBP	1200°C	100 (brittle)	8%
	$3Al_2O_3{\cdot}2SiO_2$ $0.1B_2O_3$	ZP	1200°C	70 (dissipative)[e] 50–100 µm	20%

[a]Nicalon®, Nippon Carbon; the volume of fiber is about to 35–40%.
[b]3M Co.
[c]TBB: tributylborate; SiAl: SiAl 084 Dynasyl ester; ZP: zirconium i-propoxide. TBP: tributylphosphate; TEOGe: tetraethoxygermane.
[d]In air, at RT or at 900°C.
[e]Fracture behaviour, fiber pull-out.
[f]Linear limit.

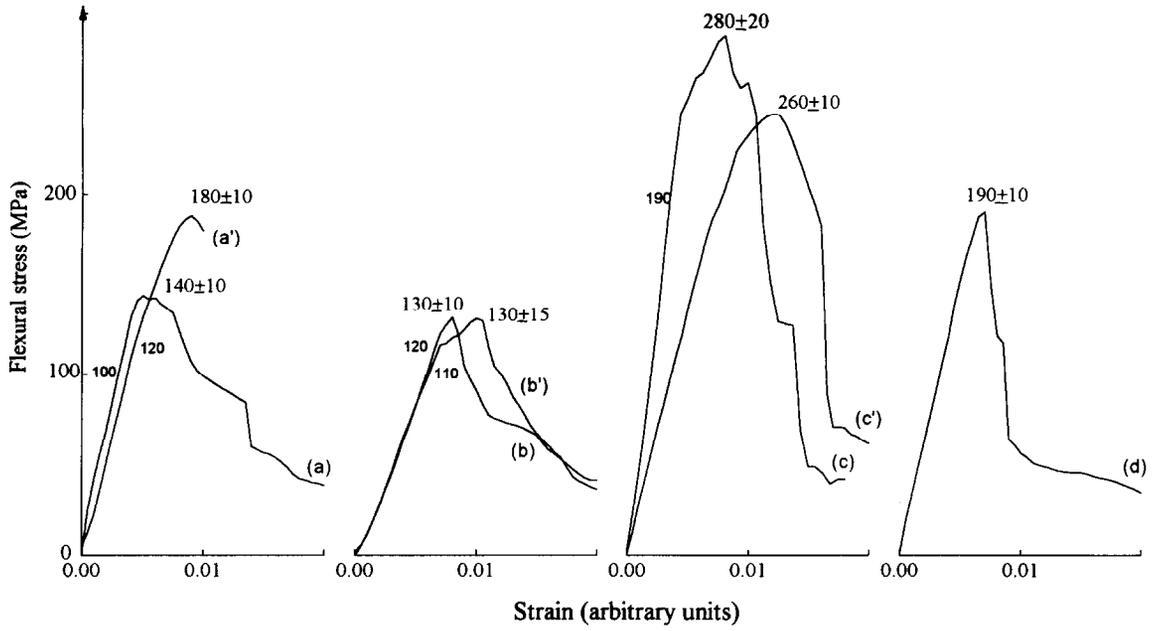

Fig. 4. Flexural stress–strain plots for various composites made with a $6Al_2O_34SiO_2ZrO_2$ matrix. Curves are recorded at RT (a, b, c, d) or at 900°C (a', b', c') in air. Samples are made with the TBB+3SiAl interface precursor, with (c, c', d) or without (a, a', b, b') addition of zirconium propoxide and tetra-ethoxygermane. The samples were sintered for 90 min at 1300°C (a, a', c, c', d) or at 1350°C with a 5 min excursion to 1450°C (b, b'). Curve d was recorded at RT after 30 h annealing at 1200°C, in air. Arbitrary relative scales are used in x-axis: the comparison is made for similar bar specimens (same number of fabrics sheets, same thickness).

the corresponding ultimate strength reaches 150 MPa at RT and at 900°C (Table 1 and Fig. 4) for zirconia containing mullite matrices. The calculated strain values are close to 0·5%. Decreasing the sintering temperature from 1350 to 1300°C is possible without increase of the porosity if the dwelling time is increased to 90 min. At the same time, the linear strength limit is increased up to 120 MPa. With the addition of ZrO_2–GeO_2 interface precursor, the densification begins below 800°C (instead of 950°C) and open porosity of ~3% is obtained after hot-pressing at 1300°C. The ultimate strength reaches 250 MPa at RT and 300 MPa at 900°C, in air. Furthermore, the equivalent strain calculated for the fibers located in the medium plane is ~0·9% at the ultimate strength which corresponds to the typical value measured for SiC fibers heated at 1200–1300°C. The linear limit is close to 180 MPa and is not lowered after 30 h annealing in air at 1200°C (Fig. 4, size of annealed samples: 35 × 5 × 4 mm). Good mechanical properties are thus observed for 2D SiC fiber and mainly tetragonal zirconia particulates–reinforced mullite matrix composites.

Mullite–mullite composites

Using mullite fiber woven fabrics, the achievement of low porosity composites without fiber–matrix reaction is much more difficult due to the high reactivity of the mullite fibers. When the interface precursor consisted of a mixture of SiAl ester and TBP as sintering aid, a rather good densification of the composite is obtained (open porosity ~8%). Neither matrix microcracking nor fiber pull-out can be deduced from the stress–strain plots (a straight line up to the failure); however fiber pull-out, typically in the range of 5–50 μm, can be observed in the fracture micrograph (Fig. 2). In order to prevent reaction between the matrix and the reinforcing fibers, we deposited an inert layer between the mullite matrix and the mullite fibers. This interphase may be selected from refractory compositions which should remain stable during the hot-pressing and at the working temperature. Thus zirconia has been chosen as interphase.

A significant work of fracture is observed on the strain–stress plot measured at samples consisting of the Nextel® 440 satin coated with ZrO_2 interphase in a B_2O_3 doped mullite matrix. X-ray diffraction patterns indicate that the zirconia interphase has monoclinic symmetry. The mechanical performances remain poor (σ ~70 MPa, Table 1) because of the high open porosity (~20%) and the low fiber volume fraction (~30%). Further work is needed to know whether the remaining porosity promotes or inhibits the dissipative character of the fracture, and to improve the mechanical strength.

Matrix, fiber and interphase characterization methodologies

The measurement of local mechanical properties is an important step in the understanding of the macroscopic behaviour of composites The indentation hardness test is probably the simplest

Table 2. Local Young's modulus (E) and Vickers microhardness (H_v) of various mullite samples and fibers

Samples	E *(GPa)*	H_v *(GPa)*	*Remarks*
$3Al_2O_3{\cdot}2SiO_2$	180 ± 17	12·4 ± 2	Hot-pressed — 1600°C (porosity <0·5%)
$3Al_2O_3{\cdot}2SiO_2$[a] with zirconia precipitates (10%, molar)	240 ± 15	16 ± 2	Hot-pressed — 1600°C (porosity <0·5%)
$3Al_2O_3{\cdot}2SiO_2{\cdot}0.1B_2O_3$ (matrix of a composite)	160 ± 20	12·5 ± 5	Hot-pressed — 1350°C (composite porosity ~12%)
$6Al_2O_3{\cdot}4SiO_2{\cdot}ZrO_2$[b] (matrix of a composite)	150 ± 20	17 ± 3	Hot-pressed — 1300°C (composite porosity ~9%)
$6Al_2O_3{\cdot}4SiO_2{\cdot}ZrO_2$[b] (matrix of a composite)	200 ± 20	18 ± 3	Hot-pressed — 1350°C (composite porosity ~9%)
$Al_2O_3{\cdot}2SiO_2$ (interphase of a composite)	90 ± 10	8 ± 2	Hot-pressed — 1350°C (composite porosity ~9%)
SiC fiber in composite pressure sintered at			
1000–1200°C	210 ± 20	25[c] ± 0·5	
1350°C	200 ± 30	20 ± 1	
1350°C[d]		17·5 ± 1	

[a]Micron dispersion; [b]Submicron dispersion; [c]Meyer law: $h = \alpha F^{\beta}$ with $\alpha = 0{\cdot}1 \pm 0{\cdot}01$ and $\beta = 0{\cdot}623 \pm 0{\cdot}03$ (F in g, d in μm); [d]a 180 min annealing at 900°C in air was performed after preparation.

method of measuring the mechanical properties of materials. The use of load-controlled depth-sensing hardness tester which operates in the (sub)micron range enables the study of each component of the composite. Following the work of Loubet *et al.*,[17] we extract Young's modulus (E) and the Vickers microhardness (H_v) from the load–displacement plot during the unloading displacement.[15] Results are given in Table 2. Typical applied load–penetration depth plots are shown in Fig. 5 for the indentation of the silica-rich interphase and of the tetragonal zirconia reinforced mullite matrix. E and H_v values are calculated using Loubet's model:

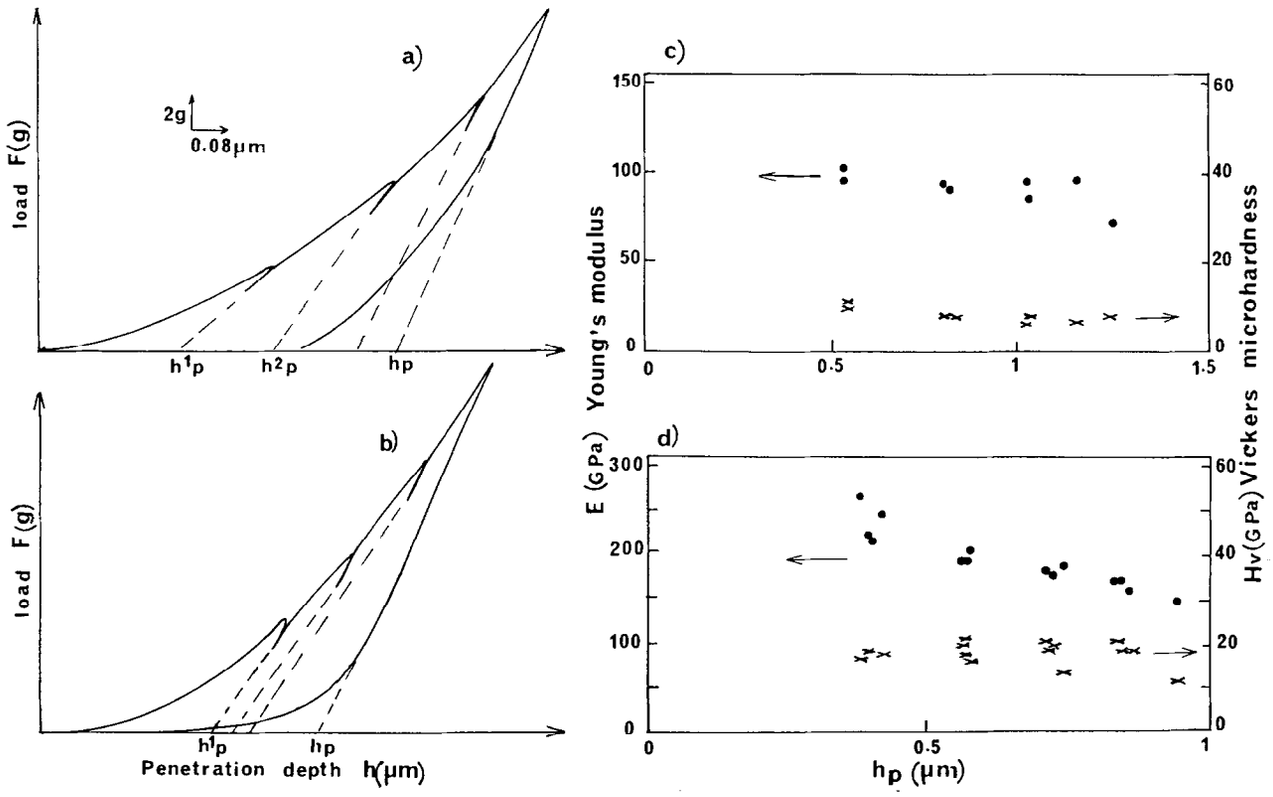

Fig. 5. $6Al_2O_34SiO_2ZrO_2$ mullite matrix; Indentation plots of applied load (F) against penetration depth (h) for (a) the fiber matrix interphase (TBB+3SiAl interface precursor, mean composition after sintering: $Al_2O_32SiO_2$) and (b) the matrix (mean composition $6Al_2O_34SiO_2ZrO_2$) region for a composite pressure sintered at 1350°C. Partial unloadings are made in order to determine the microhardness H_v and the Young's modulus E for different loads as described in Ref. 15. The H_v and E values are deduced from the plateau observed in the plots given in (c) and (d) for the interphase and the matrix, respectively.

$$E = \frac{\partial F}{\partial h}\left(\frac{\pi}{2}\right)^{1/2}\frac{1}{2\sqrt{2h_p}\tan\theta} \text{ and } H_v = \frac{F\cos^2\theta}{4h_p^2\sin\theta}$$

2θ being the angle of the Vickers pyramidal indenter and h_p the plastic depth deduced from the intersection between the extrapolation of the straight line occuring when the load is lowered (unloading cycle) and the abscissa. At very small penetration depth the measurement error is large due to the diamond tip defect and the difficulty of determining the contact point ($F = 0$ origin). At high penetration depth cracks may occur deforming the unloading trace.[15] Thus the observation of a plateau is needed to determine the true E and H_v values (Fig. 5 (c,d)).

Comparison is made with pure mullite and zirconia reinforced mullite monolithic ceramics hot-pressed at 1600°C for 1 h (Table 2). The local mechanical properties of mullite matrices sintered at 1350°C are very similar to those of dense hot-pressed monoliths. A large increase in the E and H_v values is observed for zirconia containing samples. The Young's modulus of the silica-rich mullite glass surrounding the fibers, arising from the thermal treatment of the alumino(boro)silicate interface precursor is much lower: ~90 GPa (H_v ~8 GPa). This low value corresponds to that usually measured for glass-ceramics.[18]

Indentation of the fiber allows one to observe the degradation of the fiber properties as a function of the processing and the thermal ageing. No degradation is evident in composites prepared below 1300°C: E and H_v values remain unchanged. On the other hand, the identation of fibers of composites sintered above 1300°C indicates a lowering of both Young's modulus and micro-hardness. Similar conclusions can be made after air annealing at 900°C (Table 2).

Examination of the indentation figures shows that fiber fractures are numerous and if the applied load exceeds the threshold load (F_s) (Fig. 6), the fiber slides within the matrix and a black circle

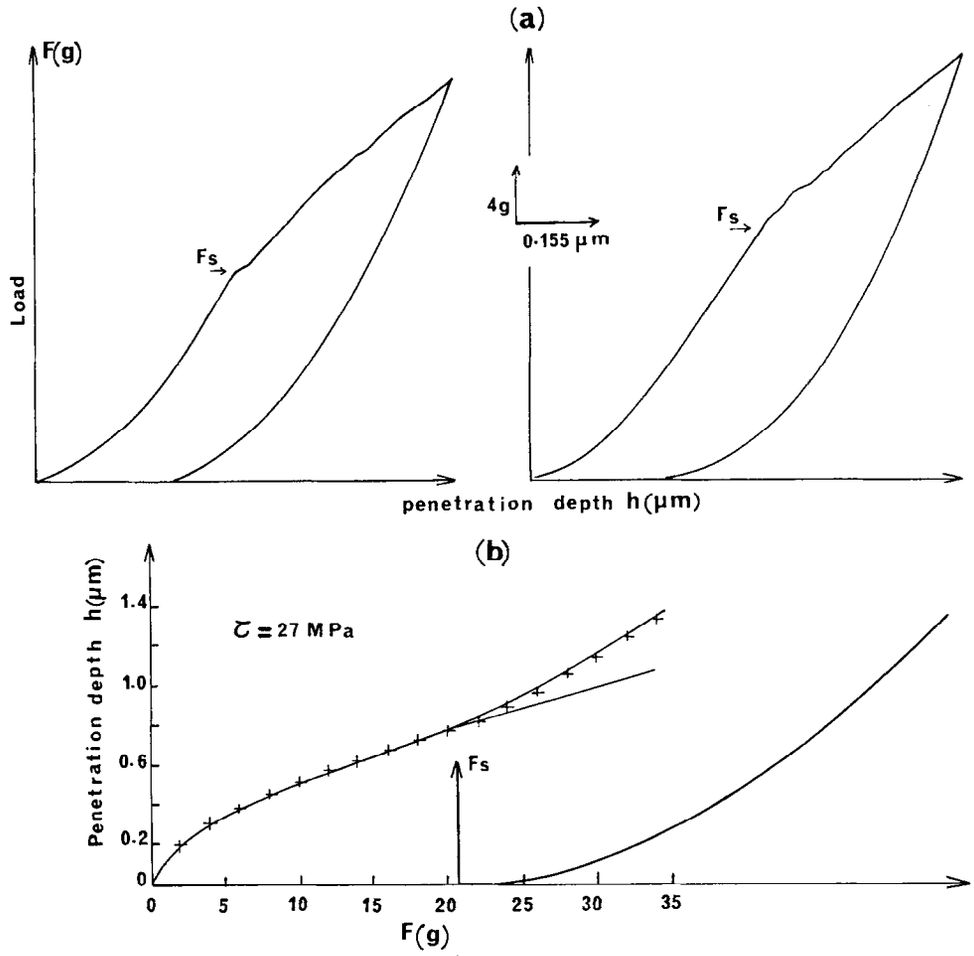

Fig. 6. (a) Typical indentation plots of applied load (F) against penetration depth (h) for various SiC fibers embedded in a silica rich–mullite glass-ceramic matrix. The steps (arrows) correspond to the debonding and the onset of the sliding regime. (b) Example of the calculation of the interfacial shear stress (τ). Crosses: experimental data from the indentation plots. Lines: calculations. The results are interpreted using a Meyer law ($h = \alpha F^{\beta}$) which describes the fiber hardness before the threshold load (F_s) plus the Marshall model in the sliding regime, after the threshold:

$$F > F_s : h = \alpha F^{\beta} + \frac{(F - F_s)^2}{4\pi^2 r^3 E\tau}$$

(E: fiber Young's modulus, r: fiber radius).

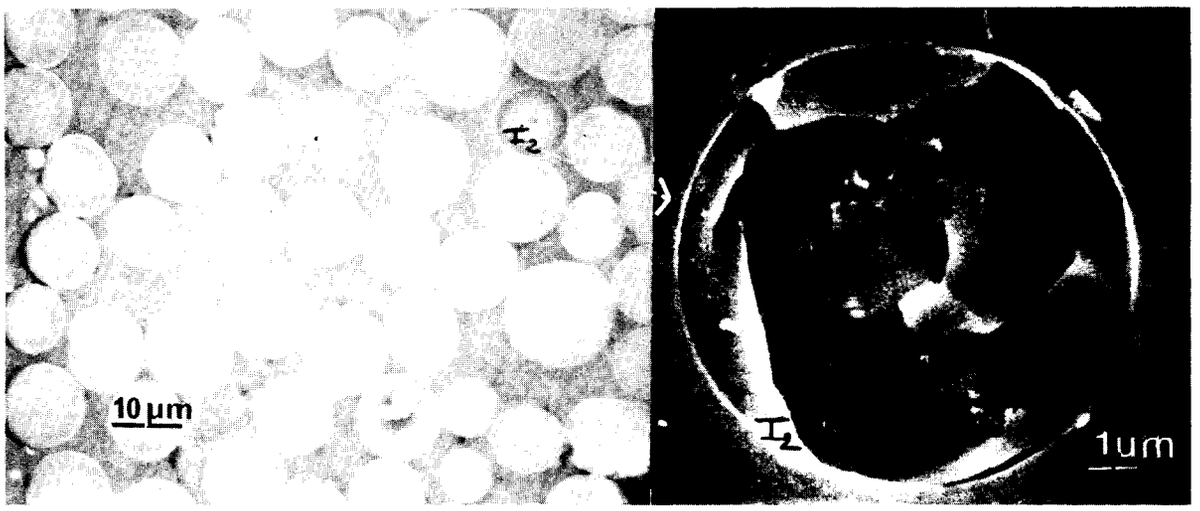

Fig. 7. SEM photomicrographs (secondary electron mode) showing SiC Nicalon® indented fibers (left); see the white contour due to the fiber debonding and the remaining step (right).

becomes visible at the fiber periphery (Fig. 7) due to the step formation: part of the fiber push-down is permanent.

Comparison of the thermal expansion coefficient measured parallel or perpendicularly to the woven fabrics gives further information about the composite. The parallel value corresponds to that imposed by the SiC fibers whereas the perpendicular value is the mean of the thermal expansion of the matrix and that of the SiC fibers. Thermal expansion coefficients are given in Table 3. A rather good agreement is obtained. No significant discrepancies are observed for zirconia-free and zirconia reinforced matrix. On the other hand, a slight shrinkage is observed above 900°C, perpendicularly, which could indicate some softening of the glassy mullite-like second phase.

Fiber/matrix interface

Figure 8 compares the line scan profiles across SiC fibers in two composites prepared using the TBB+3SiAl interface precursor with or without the addition of the ZP+TEOGe interface precursor. In both cases, we observe that some aluminium ions replace silicon ions at the fiber periphery (penetration depth ~3 μm after 45 min sintering at 1350°C). Germanium is present in the fiber periphery.

Typical transmission electron microscopy thin film micrographs are shown in Fig. 9. Four interphases are found in the interfacial region. The SiC fiber (phase no. 1) is identified by its typical electron diffraction pattern which exhibits the 111, 220 and 311 rings of the cubic βSiC structure. EDX spectra show a 5% atomic aluminum concentration. This result confirms the 'macroscopic' electron microprobe analysis of Fig. 8. The fiber crust near the interface is enriched in oxygen and depleted in silicon and carbon. Moreover, we notice in Fig. 8 that the oxygen peak of the macroscopic line scan is more intense at the fiber periphery corresponding to the Si depleted region. This indicates a superficial oxidation of the fiber. At a very fine scale the transmission electron microscope image shows an external (phase no. 2), amorphous layer of several tens of nanometers

Table 3. Mean thermal expansion coefficients (α) of 4 dir SiC fiber[a]–mullite matrix composites

Sintering[b] *temperature*	*Open porosity (%)*	$\alpha_{25\ 800°C}$ ($10^{-6}C^{-1}$)		$\alpha_{25\ 1000°C}$ ($10^{-6}C^{-1}$)	
		//	⊥	//	⊥
1300[c]	12	3·7	3·2	3·7	2·6
1350[d]	13·5	3·5	3·1	3·4	2·3
1300[e] (30 h in air at 1200°C)	3	4	—[f]	3·8	—[f]

[a]Nicalon NLM202®, the fibers are woven along four directions in a plane.
[b]Dwell-time: 30 min.
[c]Matrix :$6Al_2O_3{\cdot}4SiO_2ZrO_2$, interface precursor: 1TBB+3SiAl (see Table 1 for definition).
[d]Matrix $3Al_2O_3{\cdot}2SiO_2{\cdot}0.1B_2O_3$, interface precursor: 1TBB+3SiAl.
[e]Matrix $6Al_2O_3{\cdot}4SiO_2ZrO_2$, 1TBB+3SiAl and ZP+TEOGe interface precursors are simultaneously used.
[f]Not measured.

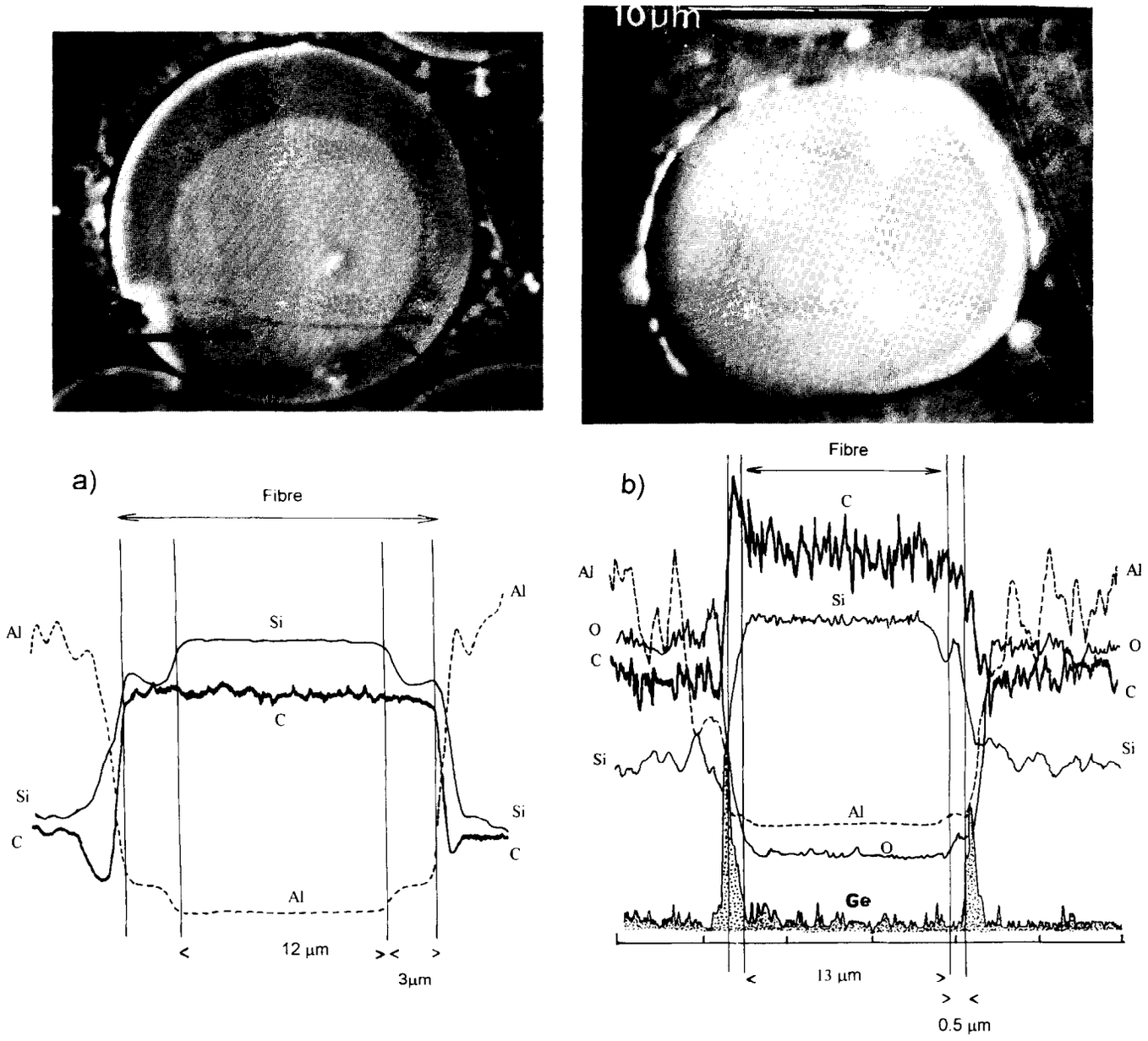

Fig. 8. SEM photomicrographs and X-ray line scan profiles recorded with a CAMEBAX electron microprobe across SiC Nicalon® fiber sections of composites prepared using the TBB+3SiAl interface precursor without (a) or with (b) addition of the ZP+TEOGe interface precursor. Al, Si, C, O, Zr and Ge profiles are measured (sintering temperature: (a) 1350°C; (b) 1300°C).

thickness. This oxide phase contains about 10 at% Al and 90% Si, respectively. Only carbon traces are detected by EDX and electron diffraction and this zone did not display the 'white' layer and the corresponding rings of graphitic carbon as observed in many other composites.[4,19–21] The interface precursor leads to small acicular $3Al_2O_3{\cdot}SiO_2$ mullite crystals (phase no. 3) dispersed in a glassy phase (phase no. 4). The composition of this last phase is 60 mol% SiO_2, 40 mol% Al_2O_3 with a relatively intense carbon signal (the size of the analyzed area is about 10×10 nm^2). The origin of the relatively high carbon content of this phase can be found in the organic traces arising from the pyrolysis of the interface precursor. Incompletely hydrolyzed branches often remain in the *in situ* gelated interface precursor. The interfaces appear to be free of a carbon film. However, these observations do not exclude the presence of a few atomic carbon planes around the SiC fibers, as observed at the interface of SiC whiskers.[22] The carbon film, if such a film is present, is thinner than that usually observed in composites made with alkali or earth-alkali-containing matrices.[19–21] Furthermore, TEM examination of the fiber/matrix interface of a composite annealed for a few hours in air at 1470°C (Fig. 9(b)) shows that the main changes are: (i) the growth of the mullite crystals; (ii) the punctuation of the SiC fiber rings which indicates the onset of the crystallization.

Fiber/matrix sliding properties

The high strength and toughness of glass-ceramic matrix composites result directly from the low

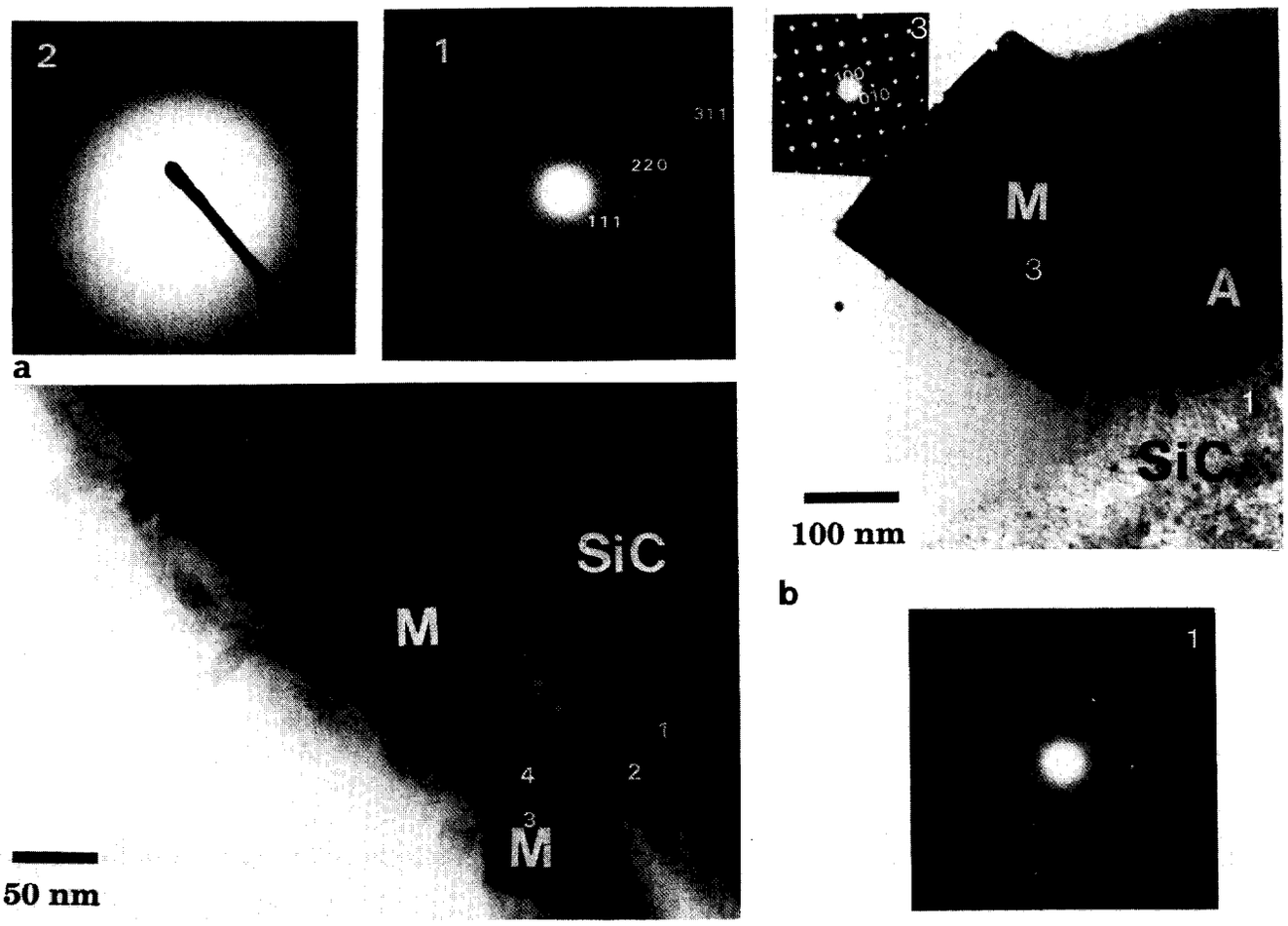

Fig. 9. TEM image of a SiC Nicalon® NLM202 fiber woven fabric-embedded in ($3Al_2O_3{\cdot}2SiO_2{\cdot}0.1B_2O_3$) mullite matrix composite elaborated using the TBB+3SiAl interface precursor and pressure sintered at 1350°C. (a) Interfacial regions are: (1) fiber; (2) external region; (3) mullite crystal: (4) amorphous aluminosilicate phase. (b) After annealing for 3 h at 1470°C, in air.

fiber/matrix bonding originates in the processing. Usually, a reaction between SiC Nicalon fibers and an alkali- or earth-alkali-containing matrix leads to the formation of a thin carbon-rich interfacial layer (~100 nm) referred to as the carbon interphase.[19–21] This interphase acts as a 'fuse', deflecting the matrix microcracks parallel to the fiber axis and thus avoiding the early failure of the fibers. This interphase is formed *in situ* during the hot-pressing as a result of the fiber/matrix chemical reaction or results from the deposit of a thin coating of C or BN when non-reactive matrices are used.[23]

Another important parameter controlling the fiber/matrix bonding is the sign and the level of the residual mechanical stresses in the composite after processing arising from the thermal coefficient expansion mismatch. Too high a radial compressive residual stress increases the fiber/matrix bonding and is usually detrimental.

The sliding strength is usually measured on 1D composites using instrumented or non-instrumented micro-hardness tester following the method of Marshall.[24–26] The fiber to be tested is selected with regard to its axial position (circular section) and to have a uniform arrangement of distances from neighbouring fibers. Its diameter is measured after indentation. If the indent is not centered or if there is the least sign of fiber splitting, the measurement is rejected. Examples of applied load indentor/tip displacement are given in Fig. 6. Three regions are clearly distinguished on the load (F)–depth (h) plots:

(i) the first polynomial regime $h = \alpha F^{\beta}$ related to the fiber indentation and its elastoplastic deformation under the sharp indenter (see above, Loubet's model, $F < F_s$),

(ii) a region characterized by a lower rate of load increase, a few steps often being observed at the limit between the elastoplastic response of the fiber and the debonding-plus-sliding regime ($F \sim F_s$),

(iii) a third region can be observed when the pyramidal diamond tip comes into contact with the matrix ($F > F_s$).

The interfacial frictional stress (τ) related to sliding may be measured in 2D material if the fiber curvature is larger than the debonding length

induced by fiber sliding. The very large yarn curvature in 4-direction woven fabrics (curvature radius > a few tens of centimetres whereas debonding length ranges between 50 and 500 μm, typically e.g. see Fig. 3) makes possible experiments and calculations.

The calculation of the interfacial stress (or sliding strength) τ is made using Marshall's uniaxial model. The elastoplastic contribution of the fiber before the sliding threshold (F_s: threshold load) is assumed to follow a Meyer law:[15]

$$h = \alpha F^{\beta} \; (\forall F \leq F_s)$$

h: penetration depth, F: applied load

In the sliding regime $\forall F > F_s$:

$$h = \alpha F^{\beta} + \frac{(F - F_s)^2}{4\pi^2 r^3 E \tau} \qquad (1)$$

E: Young's modulus, r: radius of the fiber, respectively.

A more accurate model has been proposed:[15]

$$h = \alpha F^{\beta} + \frac{F^2 - F_s^2}{4\pi^2 r^3 E \tau} \qquad (2)$$

This last model gives a τ-value 2–3 times larger than that calculated from model 1. In fact, it is very difficult to determine the true interfacial frictional stress and to compare the τ values calculated by different authors. Only comparative studies using the same model—and the same apparatus—are significant. The main results are summarized in Table 4 and typical curves are shown in Fig. 6. Comparison of the experimental data with the calculation (model no. 1) shows a rather good agreement. A similar agreement is obtained using model no. 2. A criterion for choosing between model no. 1 and model no. 2 is the height of the residual step after indentation.[15] However, the measurement is difficult and the thermally induced stress should also be taken into consideration.[26] Our τ values may be considered as comparative data. The τ value is rather constant whatever the sintering temperature (1350–1450°C temperature range). On the other hand, the threshold load is lowered when zirconia reinforced mullite is used as matrix. Comparison with experiments (using the same model and instrument) on SiC/LAS (or MLAS) matrix composites shows that our F_s values remain large (τ_{LAS} ~3–8 Mpa). The fibers can be initially debonded in the LAS (MLAS) matrix ($F_2 \leq 2$ g).[15] A large increase in the τ value is observed after annealing in air. This is consistent with the decrease in the area of the strain–stress plot (Fig. 4) and with the TEM examination: the fiber/matrix boundary is well-defined in the 1350°C sintered sample whereas a corrugated front is observed in the sample annealed for 3 h at 1470°C (Fig. 9). Benoit *et al.*[27] have demonstrated that the interface sliding behaviour is controlled by the difference between the roughness induced misfit and the thermally induced gap. The lack of a visible C film in our SiC-mullite composites could explain why our τ values remain 4–5 times larger than those measured on composites exhibiting a well-defined carbon-rich interface (e.g. SiC/LAS matrix composite). This also explains why the thermally induced degradation is slower in SiC/mullite composites than for example in SiC/LAS composites.

Thermal degradation of the matrix and fiber/matrix interphase

TEM investigation and microindentation analysis have demonstrated that the fibre–matrix interface changes after thermal annealing. Transformations are also seen in the matrix. Figure 10 shows micro-Raman spectra recorded in different places for a germanium containing composite annealed for 30 h at 1200°C in air. This annealing being performed on a very small sliced rod, it represents a brutal thermal ageing. After annealing, we observe that zircon ($ZrSiO_4$) replaces the (tetragonal and monoclinic) zirconia precipitates in the matrix. The complete disappearance of tetragonal zirconia indicates that the smaller grains have been first transformed into zircon, even though the heating temperature is lower than the usual limit for the reaction mullite + zirconia → zircon + alumina (> 1300°C). The germanium phase exhibiting the strong 300 cm^{-1} Raman peak remains present (white

Table 4. Interfacial shear stress (τ) and threshold load (F_s) of SiC fiber/mullite matrix composites[a]

Matrix	*Sintering temperature*	F_s *(g)*	τ_1^c *(MPa)*	τ_2^c *(MPa)*
$3Al_2O_3{\cdot}2SiO_2{\cdot}0.1B_2O_3$	1350°C	15–25	20 ± 5	~50
$6Al_2O_3{\cdot}4SiO_2{\cdot}ZrO_2$	1350°C	10–18	22 ± 5	~50
	+2 h		≥80	≥200
	at 900°C in air			
	1450°C	15–25	24 ± 7[b]	~50

[a]At least 12 fibers are studied.
[b]Many fibers are crushed under indentation
[c]τ_1: model of eqn (1); τ_2 model of eqn (2).

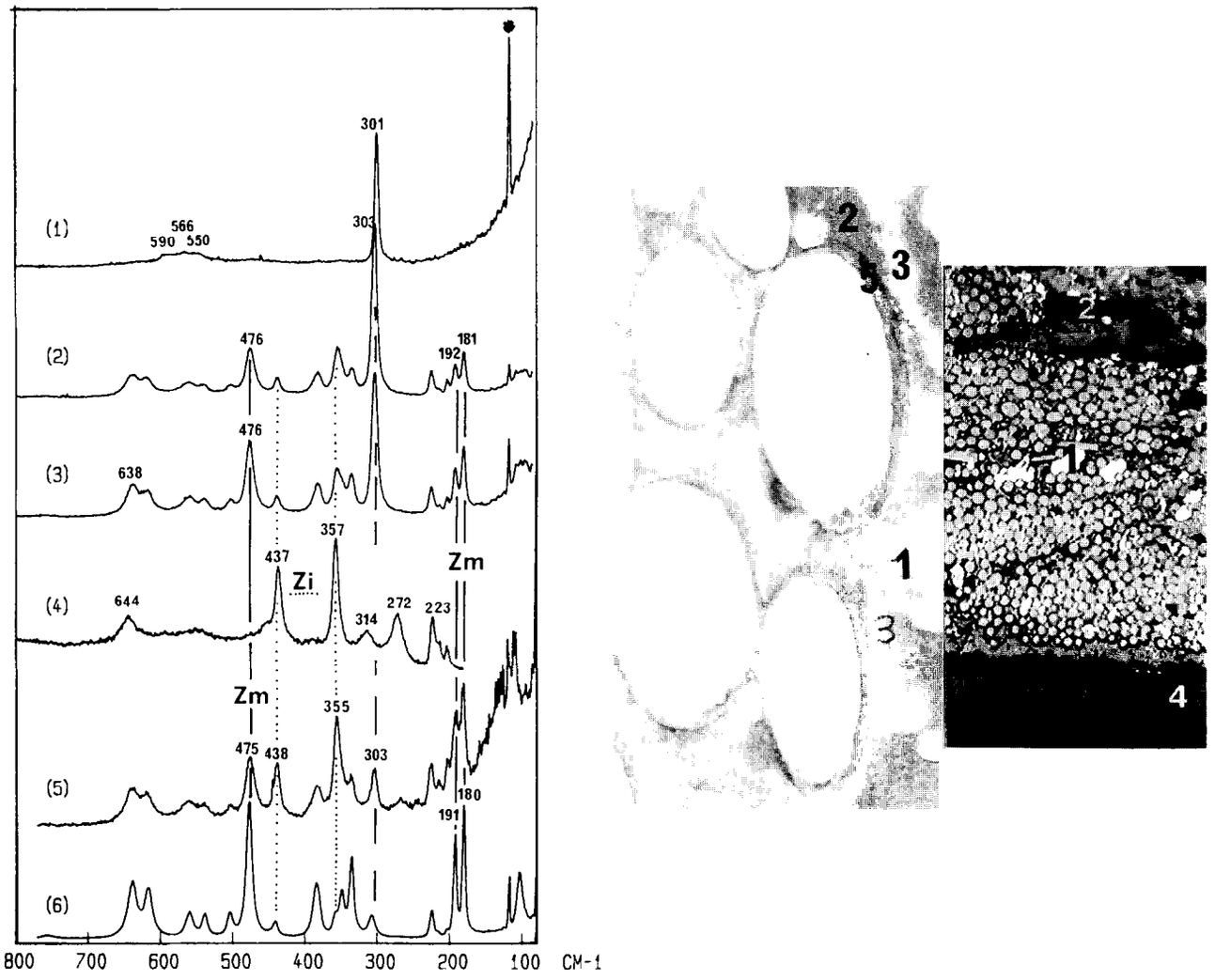

Fig. 10. Optical photomicrographs showing the reaction contour at the SiC fiber periphery in composite prepared using the ZP+TEOGe interface precursor and annealed for 30 h at 1200°C in air. The corresponding micro-Raman spectra are given: (1) Ge rich 'white' precipitate; (2) black region (main phases: Ge+Zm+Zi); (3) grey region (Zm+Zi+Ge); (4) matrix surface (Zi); (5) region around the fiber. Zm: monoclinic zirconia, Zi: zircon; (6) comparison is made with Raman spectra recorded before annealing or after annealing below 800°C (star: laser line).

grains). The interphase at the fiber contour is made of monoclinic zirconia and of zircon. This zircon crust can be formed by reaction with silicon evolving from the fiber as observed in many composites.[4]

Conclusions

From the results which have been presented and discussed the following conclusions can be drawn:

(i) Almost fully dense woven fabric mullite matrix composites have been prepared by a prepreg sol–gel route using tailored interface precursors compatible with SiC Nicalon NLM202® and/or mullite Nextel 440® fibers. Low porosity SiC-mullite composites are obtained with the help of transient liquid sintering aids (first a B_2O_3 rich phase and then a Ge/GeO_2 containing phase). The porosity of oxide fiber/mullite composites remains high and further work must be done to improve their densification.

(ii) In the as-processed composite the matrix composition changes gradually from the intersheet region to the fiber environment due to the use of two kinds of precursors, the interface and the matrix precursors. This accommodates the thermal expansion coefficient mismatch. Multilevel reinforcement is achieved (fibers, particulates).

(iii) Good (bending) mechanical properties are obtained for SiC/mullite composites (~300 MPa at RT and at 900°C). The high linear limit (180 MPa) is maintained after 30 h annealing in air. However, a gradual transformation of the zirconia precipitates into zircon is observed. The mechanical properties of mullite–mullite composites show the potential interest of such materials in air if the porosity can be lowered.

(iv) The SiC Nicalon NLM202® fiber/silica-rich mullite interphase appears to be free of a carbon film. This behaviour is consistent with the rather good preservation of sliding behaviour at the fiber/matrix interface after air annealing. On the other hand the interfacial shear stress is 3–4 times larger than that measured when the usual carbon interface is present (e.g. SiC/LAS composite). These carbon-film-free SiC-mullite composites as well as the mullite–mullite composites are promising materials for structural applications at medium temperature in an oxydizing atmosphere.

Acknowledgements

Dr D. Michel is kindly acknowledged for his help for the TEM examination. Dr M. Parlier is acknowledged for fruitful discussions.

References

1. Colomban, Ph., *Ceramics Int.*, **15** (1989) 23–50.
2. Klein. L. C., *Sol–Gel Technology*, Noyes Publication, New Jersey, 1988.
3. Colomban, Ph. & Mazerolles, L., *J. Mater. Sci.*, **26** (1991) 3503–10.
4. Bruneton, E., Michel, D. & Colomban, Ph., *J. de Physique IV*, **C7** (1993) 1937–40.
5. Guney, V., Jones, F. R., James, P. F. & Bailey, J. E., *Int. Phys. Conf. Ser. III*, IOP Publishing Ltd, 1990, pp. 217–26; Chen, M., Jones, F. R., James, P. F. & Bailey, J. E., *ibid.* 227–37.
6. Qui, D. & Pantano, C. G., *3rd Int. Conf. Ultrastructure Processing of Ceramics, Glasses and Composites*, eds J. D. Mackenzie & D. R. Ulrich, 1987, pp. 635–44.
7. Colomban, Ph. & Mouchon, E., *High Temperature Ceramic Matrix Composites*, Proc. HT-CMC1, 20–24 Sept. 1993, Bordeaux, eds R. Naslain, J. Lamon & D. Doumeingts, Woodhead Publ. Ltd, Abington, Cambridge, 1993, pp. 159–66.
8. Colomban, Ph. & Vendage, V., *J. Non-Crystalline Solids*, **147/148** (1992) 245–50.
9. Colomban, Ph., Menet, M., Mouchon, E., Courtemanche, C. & Parlier, M., French patent 2672283 (1991), European patent 92400235.5, US patent 07/8303510.
10. Prewo, K. M., *Ceram. Bull.*, **68** (1989) 395–401; Lipowitz, J., *ibid.* **70** (1991) 1888–92.
11. Colomban, Ph., *Ceramics Today–Tomorrows Ceramics*, ed. P. Vencenzini, Elsevier, Amsterdam, 1991, pp. 599–605.
12. Colomban, Ph. & Mouchon, E., *Solid State Ionics*, **73** (1994) 209–20.
13. Colomban, Ph., *J. Mater. Sci.*, **24** (1989) 3011–20.
14. Low, I. M. & MacPherson, R., *J. Mater. Sci.*, **24** (1989) 926–35.
15. Lagrange, J. L., Passilly, B., Parlier, M. & Colomban, Ph., *Proc. JNC-8 (8èmes Journées Nationales sur les Composites)*, 16–18 Nov. 1992, Palaiseau, France, eds O. Allix, J. P. Favre & P. Ladevèze, AMAC, Paris, 1992, pp. 241–52.
16. Parlier, M., Grenier, T., Renevey, S., Passilly, B., Mouchon, E., Bruneton, E. & Colomban, Ph., *Proc. 4th Int. Symp. on Ceramic Materials and Components for Engines*, 10–12 Jun. 1992, eds R. Göteborg, Carlsson, T. Johansson & L. Kahlmann, Elsevier Appl. Sci. Ltd, UK, 1992, pp. 440–8.
17. Loubet, J. L., Georges, J. M., Marchesini, O. & Meille, G., *J. Tribology*, **106** (1984) 43–8; Loubet, J. L., Georges, J. M. & Meille, G., *Microindentation Techniques in Materials Science and Engineering*, eds J. P. Blau & B. R. Lawn, ASTM STP 889, Philadelphia, 1980, pp. 72–89.
18. Ashcroft, I. A., Lawrence, C. W., Weihs, T. P. & Derby, B., *J. Am. Ceram. Soc.*, **75** (1992) 1284–6.
19. Cooper, R. F. & Chyung, K., *J. Mater, Sci.*, **22** (1987) 3148–60.
20. Brennan, J. J., *Fiber-reinforced Ceramic Composites, Materials, Processing and Technology*, ed. K. S. Mazdiyasni, 1990, pp. 223–59; Colomban, Ph. & Mouchon, E., *High Temperature Ceramic Matrix Composites*, Proc. HT-CMCI, 20–24 Sept. 1993, Bordeaux, eds R. Naslain, J. Lamon & D. Doumeingts, Woodhead Publ. Ltd, Abington, Cambridge, 1993, pp. 269–83.
21. Bleay, S., Scott, V. D., Harris, B., Cooke, R. G. & Habis, F. A., *J. Mater. Sci.*, **27** (1992) 2811–22.
22. Lin, F., Moriels, T., Morrone, A. & Nutt, S., *Mat. Res. Symp. Proc.*, **120** (1988) 323.
23. Naslain, R., *JNC-8 (8èmes Journées Nationales sur les Composites)*, 16–18 Nov. 1992, Palaiseau, France, eds O. Allix, J. P. Favre & P. Ladevèze, AMAC, Paris, 1992, pp. 199–212.
24. Marshall, D. B., *J. Am. Ceram. Soc.*, **67** (1984) C259–60.
25. Marshall, D. B. & Evans, A. G., *J. Am. Ceram. Soc.*, **68** (1985) 225–31.
26. Sudre, O., Passilly, B. & Parlier, M., *Proc. 17th Ann. Conf. Composites and Adv. Ceramics*, Cocoa Beach, Fl, 10–15 Jan. 1993, *Ceram. Eng. Sci. Proc.*, (1994), July–August, 1994, pp. 180–7.
27. Benoit, M., Brenet, P. & Rouby, D., *High Temperature Ceramic Matrix Composites*, Proc. HT-CMC1, 20–24 Sept. 1993, Bordeaux, eds R. Naslain, J. Lamon & D. Doumeingts, Woodhead Publ. Ltd, Abington, Cambridge, 1993, pp. 329–36.